UDC 543 . 5 : 669 . 15' 782

Technical Report

Characterization of Oxidation Behavior at Fe-Si Alloy Surface

Katsuyuki YANAGIHARA* Shuichi YAMAZAKI

Abstract

Oxidation behavior of Fe-Si alloys strongly depends on oxygen potential of an annealing atmosphere. In the present study, X-ray diffraction, Auger electron spectroscopy, X-ray electron photoelectron spectroscopy, glow discharge optical emission spectrometry and transmission electron microscope have been applied to characterize the microscopic features of oxides formed on an Fe-3mass%Si alloy. The samples were oxidized at 850℃ under a 75%H_2-25%N_2 atmosphere with various partial pressures of water vapor. The macroscopic results of an oxidized Fe-3mass% Si alloy agree well with prediction based on the thermodynamic data of oxidation of elements. The oxidation in higher oxygen potential generates the surface roughness and Fe layer, which caused by the internal oxidation. In case of SiO_2 film forms on the surface in early stage of oxidation, the internal oxidation is suppressed in the next stage. Consequently, internal oxidation occurs locally and it causes large surface roughness.

1. Introduction

Demand for better formability and surface properties are increasing for high-tensile steels for automotive and structural applications. The addition of Si is a well-known measure for improving the formability and strength of steel. Electrical steel sheets for the cores of motors and transformers often contain Si in amounts of about 3 mass % or less. While it has been empirically known that oxidation during production processes significantly affects the properties of these products, little has been clarified about the oxidation of steel containing Si.

Regarding oxidation of Fe-Si alloys at high temperatures, while there have been many study reports on the oxidation of high-tensile steel sheets or plates containing Si under high oxygen potential in relation to scale generation in reheating furnaces for hot rolling,[1-3] the number of reports on the oxidation of such steels under low oxygen potential is comparatively limited.[4-8]

Let us look at some of these examples. Morito and Ichida[5] studied the internal oxidation of steels containing about 3 mass % Si, and reported that the addition of Mn in amounts of 0.5 mass % or less would accelerate internal oxidation. They also reported that, when the P_{H2O}/P_{H2} ratio of the furnace atmosphere was 0.03 or less, internal oxidation zones would disappear and a film of SiO_2 would form on the surface. Yamazaki[6] theoretically explained the transition between internal and external oxidation of Fe-Si alloys. Yanagihara et al.[7] examined the oxidation of an Fe-3-mass-% Si alloy in detail, identified oxidation products, and reported changes in the surface conditions due to oxidation. Suzuki et al.[8] examined selective oxidation during recrystallization annealing of steels containing Si and Mn from a thermodynamic viewpoint, and clarified the relationship between the oxygen potential of the furnace atmosphere and the reaction paths of oxidation as well as the relationship between steel chemistry and the reaction paths.

As reported in those papers, when Fe-Si alloys oxidize under a low oxygen potential where oxides of Fe systems do not form, a very thin oxide film having a thickness in the order of nanometers forms on the surface in some cases, and in others, an internal oxide zone forms to a depth of several micrometers. To clarify the oxida-

* Chief Researcher, Materials Characterization Research Lab., Advanced Technology Research Laboratories
20-1, Shintomi, Futtsu, Chiba

tion behavior of Fe-Si alloys in a wide range of oxygen potentials, it is therefore necessary to analyze it using a variety of analysis techniques in combination.

The present report aims to clarify the oxidation of an Fe-3-mass-% Si alloy employing various surface analysis methods.

2. Analysis Method

2.1 Specimens

Sheets of an Fe-3-mass-% Si alloy after secondary recrystallization in a hydrogen atmosphere, 0.23 mm in thickness, and having an average crystal grain size at the surfaces of roughly 10 mm were used as specimens for the test, this specimen sheet hereinafter being called Sample A. **Table 1** shows the principal component elements of Sample A. The steel sheets were then oxidized in a 75%H_2-25%N_2 atmosphere for 300 s at a soaking temperature of 850℃. Here, the oxygen potential of the furnace atmosphere was changed by adding different amounts of H_2O so that the dew point was as listed in **Table 2**; the sheets oxidized under the listed dew points are hereinafter referred to, respectively, as Samples B to G.

2.2 Analysis

The phases forming after the oxidation were identified by X-ray diffraction (XRD) analysis using the characteristic X rays of Cu-K α by the $2\theta/\theta$ method. The material structure was observed at surfaces and sections using a scanning electron microscope (SEM) under the condition of an electron beam accelerating voltage of 10 kV and a current of 1 nA. The chemical composition was analyzed at the specimen surfaces by Auger electron spectroscopy (AES) and X-ray photoelectron spectroscopy (XPS). In the AES, which was performed at prescribed points, the electron beam accelerating voltage was 10 kV, and the current was 10 nA. The monochromatized characteristic X rays of Al-K α were used for the XPS analysis of areas of 200 μm squared each. Elementary distribution was analyzed from the surface to a depth of about 7 μm in a round area of about 4 mm in diameter using high-frequency glow discharge optical emission spectrochemical analysis (GD-OES). In addition, the structures of internal oxidation zones were observed, their chemical composition analyzed, and the phases identified using a transmission electron microscope (TEM) at an accelerating voltage of 200 kV.

3. Results

Fig. 1 shows the XRD profiles of the samples after oxidation. The samples that were oxidized in an atmosphere of P_{H_2O}/P_{H_2} ratios lower than that of Sample E exhibited peaks only of Fe, as was the case with Sample A; the peaks especially of Fe110 in the BCC structure near $2\theta = 44.7^\circ$ were extremely strong. This is because crystal grains selectively grew very coarse through secondary recrystallization. Sample F demonstrated peaks of Fe_2SiO_4 together with those of Fe, and Sample G, peaks of Fe, Fe_2SiO_4, and FeO.

Table 1 Chemical compositions of sample A (mass%)

C	Si	Mn	Cr	Sn	Fe
0.0018	3.16	0.08	0.03	0.12	bal.

Table 2 Samples oxidized under annealing conditions of different dew points or p_{H_2O}/p_{H_2} ratios

Sample	B	C	D	E	F	G
Dew point (℃)	-15	0	25	40	65	71
p_{H_2O}/p_{H_2} ratio	0.0022	0.008	0.04	0.10	0.43	0.63

Fig. 2 shows secondary electron images of the surfaces of Samples B, C, D, and E, and **Fig. 3** shows the AES spectra taken at Points 1 to 6 specified in Fig. 2. Note here that the downward arrow in Fig. 2 shows the rolling direction in the cold rolling of the specimen sheets. Because there were hydrocarbons and many other impurities on the sheet surfaces after the oxidation process, the sheets were cleaned through pre-sputtering with Ar^+ ion beams before AES analysis.

The surface structure of Sample B was substantially the same as that of Sample A, the surfaces of the two being flat and smooth. As seen with the curve of Point 1 in Fig. 3, the spectra of Si and O were detected at the surface of Sample B, which indicates that nearly pure SiO_2 covers the sheet surface, not in islands but in the form of a film. In Sample C, the grooves in the rolling direction, which were seen also in Sample B, were more pronounced. In addition, there were hemispherical protrusions roughly 500 nm in diameter (Point 2, etc.); judging from the results of AES analysis, they were most likely oxides of Mn-Si. The smooth portion of the surface of Sample C was covered with a film of nearly pure SiO_2.

On the surface of Sample D, there were ridges and long, flat areas running in the rolling direction; of all the samples of the present study, it had the most uneven surface. Whereas the spectra of Fe, Si, and O were detected at the top faces of the ridges (Point 4), only those of Si and O were found at the flat lower portion, which seems to indicate that the lower portions are covered with a film of nearly pure SiO_2. The entire surface of Sample F was just like the top faces of the ridges of Sample D. As seen with the curve of Point 6 in Fig. 3, only the spectra of Fe and O were obtained there; the surface was presumably covered with a film of iron oxide.

Fig. 4 shows the chemical analysis results of the sample surfaces obtained through the XPS. Like the AES analysis, the XPS analysis was conducted after pre-sputtering with Ar^+ ion beams to remove impurities on the sample surfaces. There was a film of Fe oxide on

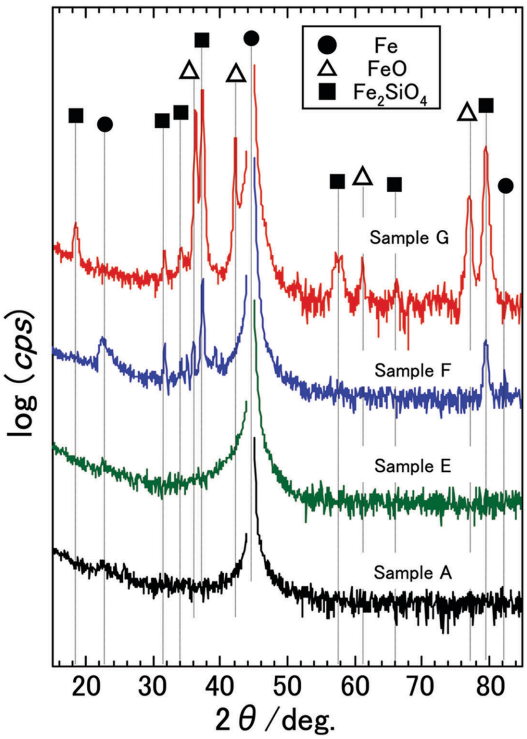

Fig. 1 XRD profiles of samples A, E, F, and G

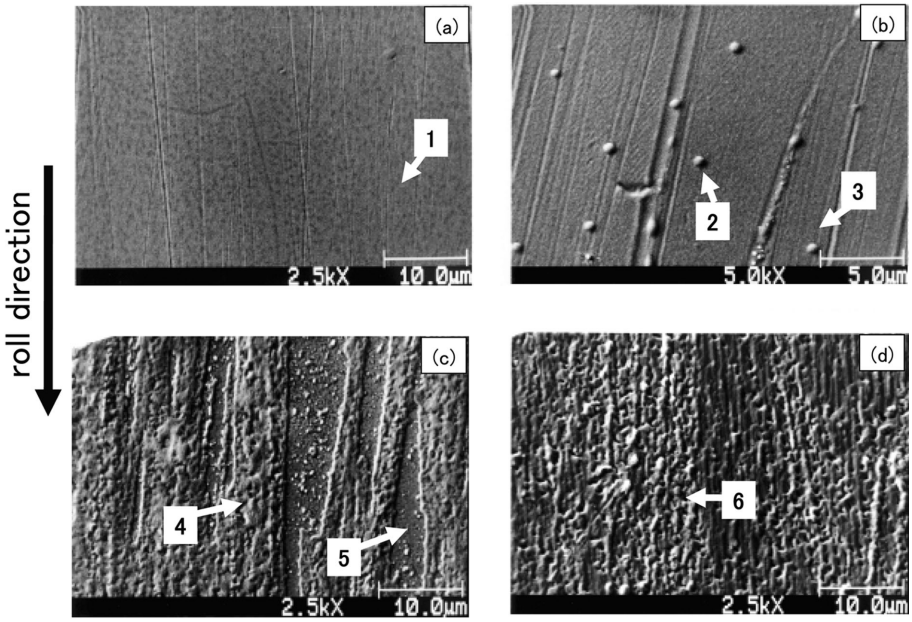

Fig. 2 Secondary-electron images of samples (a) B, (b) C, (c) D and (d) F

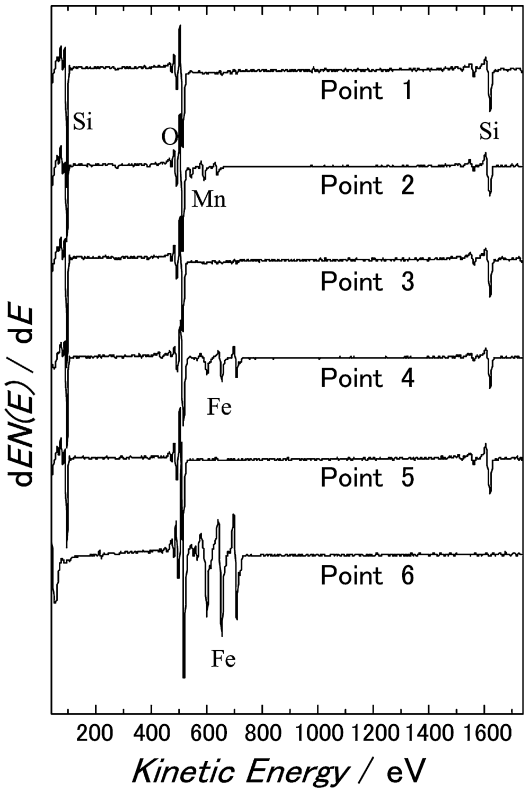

Fig. 3 AES spectra from points1-6 as denoted in Fig. 2

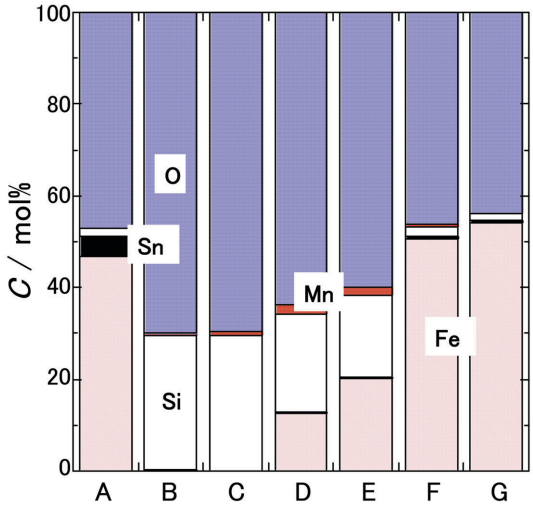

Fig. 4 Average surface composition of samples obtained by XPS analysis

the outermost surface of Sample A, and oxidized Sn accounted for about 10 mass % of the total. This Sn probably segregated at the surface during the annealing in a hydrogen atmosphere and the cooling thereafter, and oxidized in the air after the cooling. On the other hand, with Samples B and C, while the spectra of Si and O were found, no spectra of Fe were found. This indicates that a film, not islands, of virtually pure SiO_2 covers the sample surface; this agrees with the result of the AES analysis. Samples D and E exhibited spectra of Si and Fe, both as oxides, which indicates that the surfaces of these samples were covered with oxides of Si and Fe. In Samples F and G, the surfaces of which were covered with oxide films of Fe, no Si spectra were detected.

At sectional observation of the samples after oxidation, whereas products of external oxidation only were found in Samples B and C and no products of internal oxidation were found, products of internal oxidation were detected in Samples D, E, F, and G. **Fig. 5** shows sectional SEM photomicrographs of Samples D and F. Here, the spherical objects looking like bubbles in the alloy layer are products of internal oxidation. The regions of internal and external oxidation are mixed with each other in Sample D, and the internal oxidation zone is not continuous. Further, the surface of the region of internal oxidation bulges out, which agrees with the image of the surface of Sample D in Fig. 2 (c), where there are long ridges and flat, smooth

areas. In Sample F, internal oxidation took place in all the surfaces, and between the surface and the internal oxidation zone, there was a layer containing a small amount of internal oxidation products. There were oxides of comparatively small size in the surface-side part of the internal oxidization zone, and the oxides grew coarse near the thickness center of the zone. In addition, near the inner front of the internal oxidization zone, oxide grains connected with each other in parallel to the surface; a continuous film of SiO_2 of about 0.5 μm in width (or thickness) formed especially at the front.

Fig. 6 shows the GD-OES depth profile of Sample F. The abscissa represents the distance from the surface converted based on the sputtering rate before oxidation. The sample has an internal oxidation zone of about 3 μm in thickness, which agrees considerably well with the result of the sectional observation shown in Fig. 5. Besides, in the surface-side part of the internal oxidation zone, there is a region containing Cr and Mn in high concentrations, and on the other side of the zone, there is another region depleted of these elements.

Fig. 7 shows a sectional TEM photomicrograph of Sample F and electron diffraction patterns at analysis Points a, b, and c. At the outermost surface, there was a layer without oxides of about 0.2 to 0.4 μm in thickness (Zone 1), which was identified as being of virtually pure Fe through energy-dispersive x-ray spectrometry analysis (EDS) and electron diffraction. At the interface between the outermost Fe layer and the internal oxidation zone, there were internal oxidation products forming a line. Judging from its shape, this interface must have been the original sheet surface before oxidation treatment, and for this reason, the outermost Fe layer presumably formed at the surface as the internal oxidation advanced. In the surface-side part of the internal oxidation zone of about 0.5 μm in width (Zone 2), there are grains of crystalline oxides appearing black in the photomicrograph; for example, arrow [a] points to $(Fe, Mn)_2SiO_4$ containing Mn, and arrow [b] points to $Fe(Fe, Cr)_2O_4$ of a spinel structure containing Cr. Within the field of view of Fig. 7, the width of Zone 2 is virtually constant, but judging from the size and morphology of $(Fe, Mn)_2SiO_4$, $Fe(Fe, Mn)_2SiO_4$ and $Fe(Fe, Cr)_2O_4$ in the surface-side part in the sectional observation through the SEM, the width of Zone

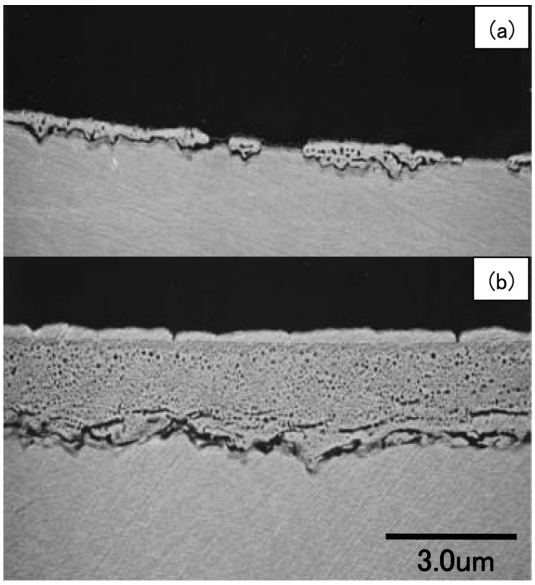

Fig. 5 Cross-section images of samples (a) D and (b) F

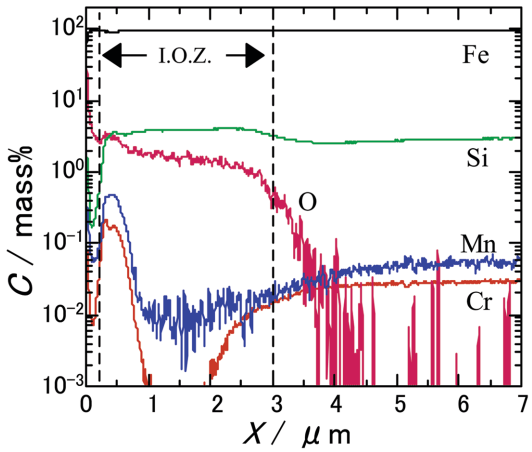

Fig. 6 GD-OES depth profile of sample F

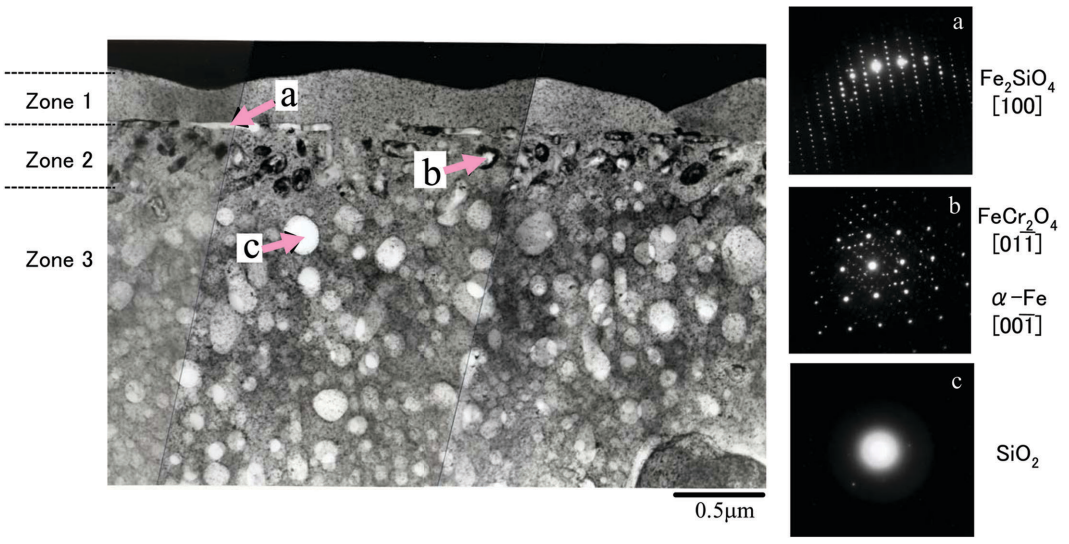

Fig. 7 Cross sectional TEM image and electron diffraction patterns of sample F

2 remains mostly unchanged in wider regions.

Zone 2 did not contain SiO_2, and all the oxides in the zone were crystalline $(Fe, Mn)_2SiO_4$ or $Fe(Fe, Cr)_2O_4$. From the results of EDS analysis of the chemical compositions of $(Fe, Mn)_2SiO_4$ and $Fe(Fe, Cr)_2O_4$, it became clear that the contents of Cr and Mn in these oxides were about 0.1 times that of Fe. Especially at the interface between Zones 1 and 2, $Fe(Fe, Cr)_2O_4$ contained Fe and Cr in nearly the same amounts. While Fe_2SiO_4 containing little Mn was found, Fe_3O_4 not containing Cr was not found. In addition, in Zone 2, Fe_2SiO_4 containing little Mn, $(Fe, Mn)_2SiO_4$ containing Mn, and $Fe(Fe, Cr)_2O_4$ were mixed with each other. On the other hand, while amorphous SiO_2 only was found in Zone 3, $(Fe, Mn)_2SiO_4$ and $Fe(Fe, Cr)_2O_4$ were not found.

4. Discussion

4.1 Thermodynamics of oxidation of Fe-Si alloy at high temperatures

Fig. 8 shows the oxygen potentials in equilibrium with different metal-oxide systems (Ellingham-type diagram). Here, the equilibrium oxygen potential with the Si-SiO_2 system is given assuming that the Si concentration in Fe is 3 mass %, and the activity of Fe and that of Mn are assumed to be 1. The following are the reactions through which FeO and Fe_2SiO_4 form.

$$2Fe + O_2 = 2FeO \quad (1)$$

$$2Fe + O_2 + SiO_2 = Fe_2SiO_4 \quad (2)$$

In relation to the above, the dew points of a 75%H_2-25%N_2 atmosphere corresponding to the equilibrium oxygen potentials for Equations (1) and (2) at 850℃ are roughly 68 and 49℃, respectively. As seen in Fig. 1, peaks of Fe, Fe_2SiO_4, and FeO were detected in Sample G, which had been prepared in an annealing atmosphere with a dew point of 71℃ and having an oxygen potential higher than the equilibrium oxygen potential of the Fe-FeO system. In Sample F, prepared in an annealing atmosphere with a dew point of 65℃ and located between the curves of Equations (1) and (2) in the Ellingham-type diagram, peaks of Fe and Fe_2SiO_4 were detected, and in the samples prepared in an annealing atmosphere whose dew point was 42℃ or lower, only peaks of Fe were detected. As seen above, in spite of the comparatively short time of soaking and oxidizing, 300 s, the XRD profiles in Figure 1 demonstrate that the oxidation of the Fe-Si alloy agrees very well with predictions based on thermodynamics.

The fact that the difference in the oxygen potentials of the annealing atmosphere between Samples C and D led to a change from external to internal oxidation agrees with results reported by Yamazaki.[6] The XRD profiles of Samples F and G confirmed the existence of Fe_2SiO_4 layers in them; however, the Si concentration was low at their surfaces and no existence of any Fe_2SiO_4 phase was confirmed there. As can be seen in Fig. 7, Fe_2SiO_4 existed in the surface-side part of the internal oxidation zone, and presumably, the Fe_2SiO_4 phase detected through XRD analysis was mainly that in the internal oxidation zone.

4.2 Activity of Mn in Fe-Si alloy

The following are the chemical reactions through which Mn solute in steel turns into MnO and $MnSiO_3$.

$$2\underline{Mn} + O_2 = 2MnO \quad (3)$$

$$2\underline{Mn} + O_2 + 2\,SiO_2 = 2MnSiO_3 \quad (4)$$

Whereas Mn in the Fe-Si alloy did not oxidize in Sample B, islands of Mn-Si oxide formed on the surface of Sample C. Assuming that pure MnO forms through the reaction of Equation (3) in a state of equilibrium, the range of $a_{\underline{Mn}}$ will be $4.36 \times 10^{-4} < a_{\underline{Mn}} < 1.58 \times 10^{-3}$. Likewise, assuming that $MnSiO_3$ forms through the reaction of Equation (4), it will be $1.42 \times 10^{-4} < a_{\underline{Mn}} < 5.16 \times 10^{-4}$. While the structure and phase of the island-shaped Mn-Si oxide were not clear, it was possible to predict that the activity of Mn ($a_{\underline{Mn}}$) in the Fe-Si alloy containing 0.08 mass % Mn used for the present study was approximately 10^{-4} to 10^{-3}, and it became clear through tests that it was nearly equal to $C_{\underline{Mn}}$.

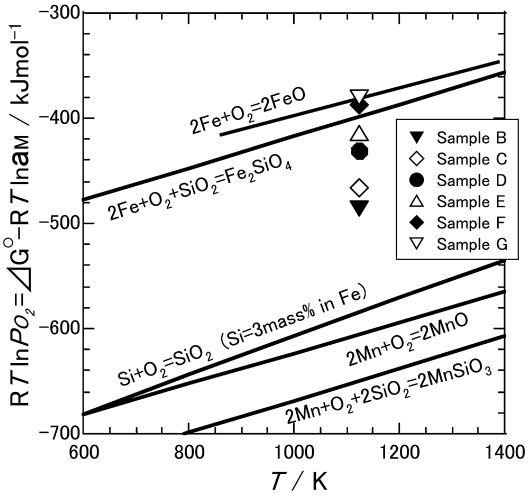

Fig. 8 Ellingham-type diagram

4.3 Change in surface structure due to internal oxidation

From the fact that nodular Ag develops on the surfaces of Ag-In alloy specimens as the internal oxidation of the alloy advances and that the total volume of the nodules is roughly equal to the volume increase due to the internal oxidation, Guruswamy et al.[9] concluded that the growth of nodular Ag resulting from the deformation of the Ag matrix by Nabarro-Herring creep was due to internal stress caused by internal oxidation. The mechanism of this seems to be very much similar to that by which an Fe layer formed on the surfaces of the Fe-Si alloy specimens in the present study as the internal oxidation advanced, as seen in Fig. 7. In other words, mainly because of the internal oxidation of Si, a strong compression stress arose in the internal oxidation zone, and as Si and other alloy elements oxidized internally, the alloy matrix changed into nearly pure iron. The mechanism by which an originally flat specimen surface thrusts upwards and a layer of nearly pure Fe forms on the surface is probably that the compression stress arising inside the internal oxidation zone serves as the driving force for the Fe matrix to creep to the surface.

4.4 Effects of surface oxidation film on internal oxidation

Whereas the internal oxidation advanced in Samples F and G more or less homogeneously in terms of depth from the surface, that in Sample D was not homogeneous. **Fig. 9** schematically illustrates the change of surface structure due to oxidation. Whether external or internal oxidation takes place depends on the competition between the flux of a solute element due to its outward diffusion and that of O due to its inward diffusion, and as a result, when the oxygen potential of the atmosphere (the dew point, in the case of the present study) is low, external oxidation becomes predominant. In this situation, if films of SiO_2 cover the surface by more than a certain proportion at the initial stage of oxidation, internal oxidation in such portions is suppressed at later stages, and as a result, external oxidation only will advance locally while internal oxidation will take place in other parts.

In contrast, when the oxygen potential of the atmosphere is high,

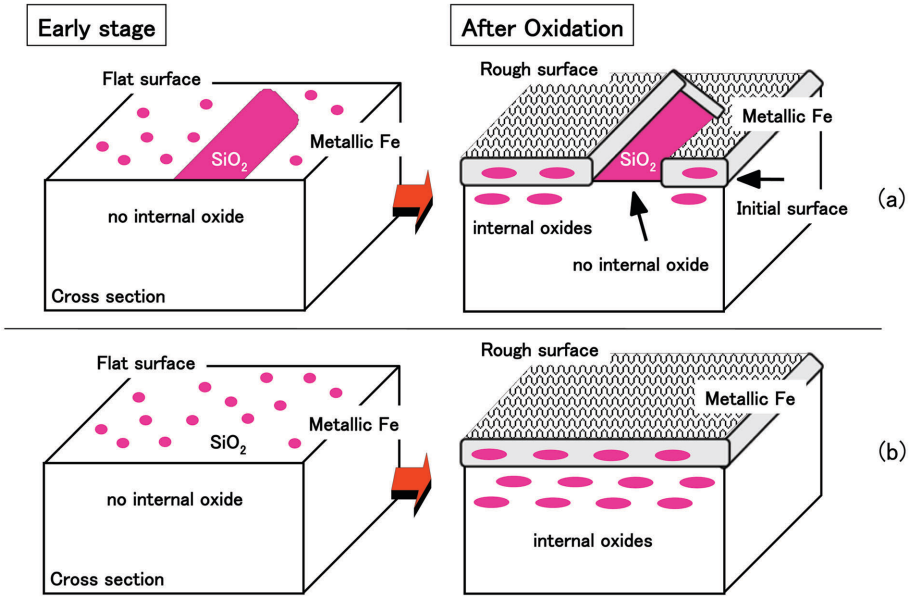

Fig. 9 Schematic surface structure of samples (a) D and (b) F caused by oxidation

Si forms fine external and internal oxides at an early stage of oxidation, and a film of SiO_2 does not form on the surface. As a result, internal oxidation will advance thereafter more or less homogeneously in the depth direction. Here, the higher the oxygen potential of the atmosphere, the larger the amount of internal oxides becomes; in fact, the content of internal oxides in Sample F was larger than that in Sample D. On the other hand, the surface of Sample F was smoother than that of Sample D. As stated in Subsection 4.3, specimen surfaces, which were flat and smooth before oxidation, became rough owing to the upthrusting resulting from the creep deformation of the Fe matrix due to internal oxidation. Because internal oxidation advanced unevenly in Sample D, its surface became more rugged than that of Sample F, in which internal oxidation took place evenly keeping the surface flat throughout the oxidation process for 300 s.

5. Closing

Sheet specimens of an Fe-Si alloy were oxidized at a soaking temperature of 850℃ for 300 s in an atmosphere containing H_2 under different dew point conditions, and the oxidized samples thus prepared were examined employing various analysis methods. As a result, the following findings were obtained:

(1) In spite of the comparatively low temperature (850℃) and the short period (300 s) of oxidizing, the oxidation mechanism of the alloy agreed very well with thermodynamic predictions.

(2) The activity of Mn (a_{Mn}) was calculated experimentally from the oxidation behavior of Mn solute in the Fe-Si alloy, and was found to be nearly equal to C_{Mn}.

(3) The Fe matrix underwent creep deformation under stress due to volume expansion resulting from internal oxidation, and as a consequence, an Fe layer formed on the specimen surface, and the surface of the specimen portion where internal oxidation took place became rugged.

(4) In the case where films of SiO_2 formed because of external oxidation and covered more than a certain proportion of the specimen surface at an early stage of oxidation, the internal oxidation in the covered portions was suppressed thereafter. This suppression of internal oxidation was notable especially in the case of oxidation treatment in a low-dew-point atmosphere, resulting in uneven advance of internal oxidation in the depth direction.

References

1) Nakamura, T., Sato, M.: Tetsu-to-Hagané. 79, 74 (1993)
2) Fukagawa, T., Okada, H., Maehara, Y.: ISIJ international. 34, 906 (1994)
3) Fukumoto, M., Hayashi, S., Maeda, S., Narita, T.: Tetsu-to-Hagané. 85, 16 (1999)
4) Block, W. F., Jayaraman, N.: Mater. Sci. Tech. 2, 22 (1986)
5) Morito, N., Ichida, T.: Corros. Sci. 17, 961 (1977)
6) Yamazaki, S.: Materia. 37, 179 (1998)
7) Yanagihara, K., Suzuki, S., Yamazaki, S.: Oxidation of Metals. 57, 281 (2002)
8) Suzuki, Y., Yamashita, T., Sugimoto, Y., Fujita, S., Yamaguchi, S.: Tetsu-to-Hagané. 96, 11 (2010)
9) Guruswamy, S., Park, S. M., Hirth, J. P., Rapp, R. A.: Oxid. Metals. 26, 77 (1986)

Katsuyuki YANAGIHARA
Chief Researcher,
Materials Characterization Research Lab.,
Advanced Technology Research Laboratories
20-1, Shintomi, Futtsu, Chiba

Shuichi YAMAZAKI
Chief Researcher,
Electromagnetic Materials Lab.,
Steel Research Laboratories